Journal of Computer-Aided Molecular Design, 5 (1991) 187–203
ESCOM

J-CAMD 118

Molecular dynamics simulation of the renin inhibitor H142 in water

Olle Teleman[a,*], Maria Lindberg[b] and Sven Engström[c]

[a]*Department of Physical Chemistry 2, Chemical Centre, Lund University, P.O.B. 124, S-221 00 Lund, Sweden*
[b]*Department of Physical Chemistry, Umeå University, S-901 87 Umeå, Sweden*
[c]*Department of Food Technology, Chemical Centre, Lund University, P.O.B. 124, S-221 00 Lund, Sweden*

Received 19 October 1990
Accepted 5 December 1990

Key words: Computer simulation; Peptide; Free energy

SUMMARY

H142 is a synthetic decapeptide designed to inhibit renin, an enzyme acting in the regulation of blood pressure. The inhibiting effect of H142 is caused by a reduction of a -Leu-Val-peptide bond (i. e. C(=O)-NH→CH_2-NH). The conformational and dynamical properties of H142 and its unreduced counterpart (H142n) was modelled by means of molecular dynamics simulations. Water was either included explicitly in the simulations or as a dielectric continuum. When water molecules surround the peptides, they remain in a more or less extended conformation through the simulation. If water is replaced by a dielectric continuum, the peptides undergo a conformational change from an extended to a folded state. It is not clear whether this difference is a consequence of a too short simulation time for the water simulations, a force-field artifact promoting extended conformations, or if the extended conformation represents the true conformational state of the peptide. A number of dynamic properties were evaluated as well, such as overall rotation, translational diffusion, side-chain dynamics and hydrogen bonding.

INTRODUCTION

The synthetic decapeptide H142 was designed to inhibit human renin, an enzyme catalyzing the conversion of angiotensinogen to angiotensin II, the latter causing elevation of blood pressure. The peptide sequence of H142 is Pro-His-Pro-Phe-His-Leu-(R)-Val-Ile-His-Lys, where R indicates that the carbonyl group in the Leu-Val peptide bond has been reduced to a methylene group, since that is the bond cleaved by renin. H142 has been cocrystallized with endothiapepsin, an aspartic proteinase belonging to the same homologous family as renin, and its 3D structure has been solved by X-ray diffraction [1]. The structure of H142 in endothiapepsin is given in Fig. 1.

Several molecular dynamics (MD) simulations on systems containing small molecules, as well

* To whom correspondence should be addressed.

0920-654X/$ 5.00

as macromolecules (e. g. proteins) in solution have been published [2–6], while studies of intermediate sized molecules, like oligopeptides, in solution are less frequent in the literature [7–13]. For small molecules it is feasible to investigate the full conformational space in simulations, while for macromolecules it is assumed that only a very small part of conformational space around some well-defined equilibrium is important. Oligopeptides, which are somewhere in between, enjoy more flexibility and it is therefore more difficult to ascertain that all relevant parts of phase space have been sampled.

On the other hand, oligopeptides receive an ever-increasing interest as drugs, since they supposedly mimic the normal substrates better, causing fewer side-effects. The MD technique is expected to be a valuable tool for the study of oligopeptides, since the method, in contrast to molecular mechanics techniques, takes entropy into account and thus is able to deal with free energy. It also provides data with respect to physical time and hence dynamical properties, as opposed to

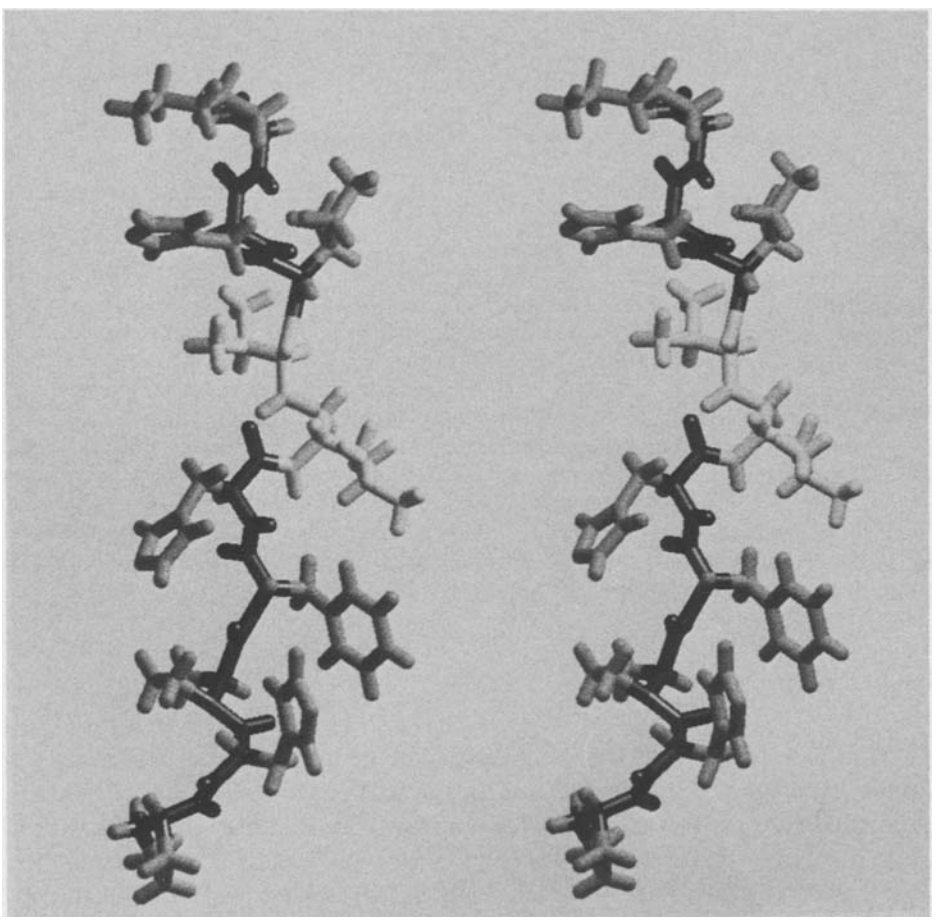

Fig. 1. The conformation of H142 in its complex with endothiapepsin. All atoms are drawn. The backbone is dark grey, the side-chains lighter grey. Leu^{6} and Val^{7} are drawn in white. The thickness of the sticks corresponds to a diameter of 0.6 Å. Coordinates for Lys^{10}, the topmost residue, were not available from the crystal study. This residue was positioned manually. The Fig. was prepared with the graphics program WINSOM, which was generously made available to us by the IBM Scientific Centre at Winchester, U.K.

Monte Carlo simulation. The drawback is that MD simulations are more time-consuming and it is relevant to ask whether the increased effort pays off in a more reliable description of the system being studied.

We have used the structure shown in Fig. 1 as a starting point for an MD study of H142 in aqueous solution. The purpose of the work was many-fold: (i) to study the structure and dynamics of H142 in water and compare the results with those obtained for the non-reduced peptide (i.e. -Leu-Val-), (ii) to compare the effects of molecular water and a dielectric continuum on the structure of H142, (iii) to compare the structural results obtained with energy minimization on one hand, and MD on the other, and (iv) to compare the MD structure in water with that obtained from 2D NMR data. So far, the last comparison has not been possible since H142 seems to aggregate in water at the concentration needed for NMR experiments.

METHODS

Interaction potential

The interaction potential is that of Ahlström et al. [14], although modified so that all atoms (including non-polar hydrogens) are treated explicitly. A recent simulation study [15] of Calbindin D_{9k}, a 75-residue protein, showed that the potential with explicit hydrogens is better able to reproduce local dynamics and certain relaxation phenomena.

The potential is based on atomic interactions. A pair of atoms i and j belonging to different molecules or separated by more than two bonds interact via a Lennard-Jones (LJ) and a Coulomb potential (Eq. 1).

$$U_{ij} = 4\varepsilon_{ij}\left\{\left(\frac{\sigma_{ij}}{r_{ij}}\right)^{12} - \left(\frac{\sigma_{ij}}{r_{ij}}\right)^{6}\right\} + \frac{1}{4\pi\varepsilon_0\varepsilon_r}\frac{q_i q_j}{r_{ij}} \tag{1}$$

ε_{ij} and σ_{ij} are the usual Lennard-Jones parameters and q_i is the partial charge of atom i. Different values for the relative dielectric permittivity were used, see below. The parameter values were based on data in the literature [16–19]; for water the SPC model was used, but with intramolecular flexibility [20].

The internal bond and bond angle vibrations were treated explicitly, and, assuming harmonicity, the potential function is given by Eq. 2,

$$U_{intra} = \sum_{bonds}\frac{k_b}{2}(x_i - x_{i,eq})^2 + \sum_{angles}\frac{k_a}{2}(\theta_i - \theta_{i,eq})^2 \tag{2}$$

where x_i and $x_{i,eq}$ are the actual bond length and the equilibrium distance, respectively, with similar notation for angles. The force constants k_a and k_b and the equilibrium values were taken from the literature [17,19,21,22]. The interactions due to internal rotation were handled by means of periodic dihedral (torsion) potentials, Eq. 3,

$$U_{int.rot.} = \sum_k\sum_n C_{k,n}\{1 - \cos(n\psi_k)\} \tag{3}$$

where ψ_k is a dihedral angle and $C_{k,n}$ an interaction parameter; k runs over all dihedral angles

at each bond. The parameters in Eqs. 1–3 are available as supplementary material to Ahlström et al. (cf. Ref. 14) or directly from the authors. No explicit hydrogen-bond potential was used; instead hydrogen bonds are assumed to be adequately described by Coulomb and Lennard-Jones terms.

Simulation technique

All simulations were done using the MD package MUMOD of Teleman and Jönsson [23] and will be described only briefly. The trajectory is a solution to the Newtonian equation of motion and was obtained numerically by means of a fourth-order predictor-corrector Gear algorithm. The program is based on independent atoms and hence includes covalent interactions in terms of harmonic and periodic potentials. This usually requires a rather small time step because of rapid bond and bond-angle vibrations. In order to circumvent this problem we have devised a two-time-step algorithm [23], where different time steps are used for slowly and rapidly varying degrees of freedom. Here, covalent bonds and bond angles were integrated with a time step of 0.2 fs (1 fs = 10^{-15} s), and all other degrees of freedom with one of 1.2 fs. The two-time-step algorithm gives radial distribution functions and translational diffusion coefficients identical to those obtained from a one-step algorithm with a time step of 0.2 fs [24]. All simulation programs are available from the authors.

Simulations were started from the conformation of H142 in its complex with endothiapepsin as determined by X-ray crystallography [1]. The crystal structure does not give the position of the Lys^{10} residue. This lysine was added manually, placing it in a position not interfering with the rest of the peptide. The pH is not well-defined in a simulation sample. The three histidines were all uncharged, which, according to an NMR titration study, corresponds to pH > 7.0 (Charlotta Jo-

TABLE 1
SIMULATIONS

Name	Peptide	Environment	Number of atoms	Equilibration (ns)	Anal.traj. length (ns)	Average temp. (K)	Average press. (MPa)
H142n(v)	H142n	continuum, $\varepsilon = 1$	178	0.0211	0.2304	311.4	0.0 ± 2.5
H142n(4)	H142n	continuum, $\varepsilon = 4$	178	0.0211	0.2304	310.6	0.1 ± 1.2
H142n(20)	H142n	continuum, $\varepsilon = 20$	178	0.0211	0.2304	309.6	0.0 ± 3.5
H142n(80)	H142n	continuum, $\varepsilon = 80$	178	0.0211	0.2304	310.9	0.1 ± 3.0
H142(v)	H142	continuum, $\varepsilon = 1$	179	0.0211	0.2304	311.4	−0.1 ± 2.4
H142(4)	H142	continuum, $\varepsilon = 4$	179	0.0211	0.2304	309.6	0.3 ± 2.2
H142(20)	H142	continuum, $\varepsilon = 20$	179	0.0211	0.2304	312.6	0.2 ± 2.4
H142(80)	H142	continuum, $\varepsilon = 80$	179	0.0211	0.2304	310.1	0.0 ± 2.8
H142n(aq)	H142n	909 H_2O, pbc	2906	0.0211	0.2506	312.2	44 ± 12
H142(aq)	H142	909 H_2O, pbc	2907	0.0211	0.2525	312.4	49 ± 2
H142(600)	H142	909 H_2O, pbc	2907	0.0019	0.0768	602.9	655 ± 26

pbc = periodic boundary conditions.

TABLE 2
SIMULATION PARAMETERS

	Continuum simulations	Aqueous simulations
Box size (Å)	∞	$31.0 \times 31.0 \times 31.0$
Time step (fs)	0.2/1.2	0.2/1.2
Velocity scaling (ps)	0.096	0.096
Sampling interval (ps)	0.48	0.48

hansson, personal communication). Lysine[10] was charged, so that the approximate pH range is 7.0–10.0, a range which includes the pH of blood, 7.4. The protonation state is given as NH_2^+ in Val[7] in the enzyme complex. In our simulations of the free peptide, the amino group was uncharged.

The peptide with a normal carbonyl group in Leu[6] instead of a methylene will be referred to as H142n. The initial conformation for H142n was identical to the H142 one, except for manual reinstatement of the ordinary peptide carbonyl group in Leu[6].

Five simulations for each peptide were run, using different environments. These runs are listed in Table 1. The simulations with explicit water, H142(aq) and H142n(aq), each contained 909 water molecules. Initially, 1000 water molecules were placed on the bases of a primitive cubic lattice of $10 \times 10 \times 10$ points with a repeat distance of 3.1 Å. Water molecules overlapping with the peptide were removed and all water orientations were randomized. Peptide and solvent filled a cubic cell with a side length of 31.0 Å, which amounts to a concentration of 56 mM, and full periodic boundary conditions were used. The other eight simulations used neither explicit water nor a periodic boundary, and we will refer to them as continuum simulations.

All simulations were equilibrated for about 21 ps (see Table 1), whereafter up to 250 ps were sampled for analysis. Below, times refer to the analysis part of the simulation only, so that 0 ps means the start of the analysis part and not the start of the entire simulation. Further, the H142(aq) run was extended by 80 ps, but at a temperature of 600 K. Simulation parameters and some averages are given in Tables 1 and 2. A total of 369 CPU hours were used on an IBM 3090–600E VF.

A further reference point for comparing the simulated conformations was obtained by generating low-energy conformations close to the starting points. As a *quasi* energy minimization, both peptides were simulated at 10 K (entropic contribution to free energy reduced by a factor of 30 compared to room temperature) for 7 ps. Even at 10 K, bad van der Waals contacts in the crystal structure data may provide the energy to drive conformational changes. Here, such changes were prevented by limiting all atomic speeds to twice the thermal speed. The acceleration and higher derivatives were limited to twice the thermal speed divided by the appropriate Taylor factor. The energy of a bad van der Waals contact is quickly converted into highly localized thermal energy and thus efficiently removed by enforcing a speed limit. The surplus thermal energy can also be removed by temperature scaling, but this leads to a temporarily unbalanced speed distribution as all speeds are scaled by the same factor. Here, temperature scaling provided the thermal bath, while the limit in speed ensured that bad van der Waals contacts did not cause unwanted conformational changes.

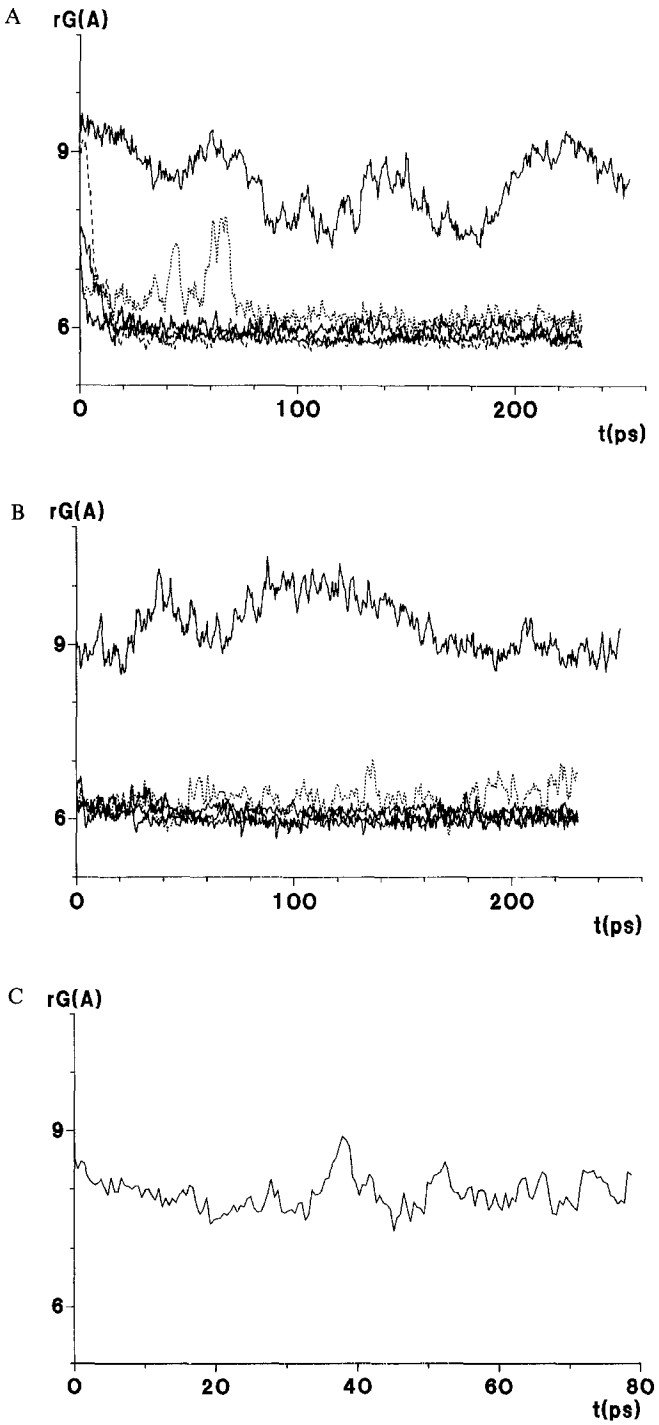

Fig. 2. Radius of gyration as function of time. A shows the data for H142(aq) (topmost line), H142(80) (dotted line), H142(v) (dashed line), H142(20) and H142(4) (2 full lines). B shows the data for H142n(aq) (topmost line), H142n(80) (dotted line), H142n(20), H142n(4) and H142n(v) (3 full lines). C shows the radius of gyration in H142(600).

RESULTS AND DISCUSSION

The present 11 trajectories were sampled rather infrequently, with a sampling interval of 0.48 ps. Even so, the obtained data amount to about 50 Mbytes, and one can obviously evaluate very many properties [25]. We will concentrate on peptide conformation as a function of model environment and chemical modification. We will also briefly discuss dynamic properties of H142, such as diffusion coefficient and internal flexibility, as such properties cannot be obtained by molecular mechanics, energy minimization or Monte Carlo simulation.

General shape was monitored by the radius of gyration and the principal moments of inertia. The radius of gyration is shown in Fig. 2. In all vacuum simulations r_G decreases and stabilizes at 6.0 ± 0.5 Å, as opposed to the value of $r_G = 9$ Å of H142 in the endothiapepsin complex. The folding is slower in the runs with higher permittivity, especially for $\varepsilon = 80$, which indicates that the folding is driven by electrostatic interactions. In the water simulations, r_G fluctuates and the peptide does not fold. H142 is, however, expected to fold in water because of the hydrophobic residues Phe[4], Leu[6], Val[7] and Ile[8], which also account for the low solubility of H142. The hydrophobic interaction governing this folding is not understood, and the only way to model it is by full simulation of the solvent. Compared to the vacuum simulations, which grossly overestimate electrostatic interactions, the solvent changes the equilibrium between folded and unfolded states towards the unfolded by screening the electrostatics and by providing peptide-solvent hydrogen bonds

TABLE 3
RADIUS OF GYRATION AND MOMENTS OF INERTIA*

	R_G (Å)	I_L (10^4auÅ^2)	I_M (10^4auÅ^2)	I_S (10^4auÅ^2)	I_L/I_M	I_S/I_M
H142(1)	5.9 ±0.5	3.6±1.2	2.9 ±0.5	2.2 ±0.1	1.24	0.78
H142(4)	6.0 ±0.3	3.8±0.5	3.0 ±0.2	2.1 ±0.2	1.26	0.70
H142(20)	5.9 ±0.2	3.6±0.3	3.0 ±0.2	1.8 ±0.1	1.21	0.63
H142(80)	6.2 ±0.1	4.0±0.2	3.4 ±0.2	1.9 ±0.1	1.19	0.56
H142n(1)	6.0 ±0.1	3.9±0.2	2.8 ±0.3	2.2 ±0.1	1.11	0.56
H142n(4)	6.1 ±0.1	4.2±0.2	3.12±0.09	1.96±0.07	1.34	0.63
H142n(20)	6.1 ±0.1	3.5±0.2	3.0 ±0.2	2.4 ±0.1	1.16	0.78
H142n(80)	6.3 ±0.2	4.3±0.4	3.7 ±0.4	1.8 ±0.1	1.17	0.48
H142(aq)	8.5 ±0.6	9.3±1.8	5.6 ±0.9	2.7 ±0.4	1.66	0.48
H142n(aq)	9.3 ±0.5	11.8±1.7	7.5 ±1.3	2.0 ±0.7	1.57	0.27
H142n(1)[a]	5.96±0.07	3.8±0.1	2.66±0.09	2.22±0.08	1.44	0.84
H142n(aq)[b]	8.9 ±0.2	10.0±0.6	8.0 ±0.7	1.6 ±0.3	1.25	0.20
H142(20)[c]	5.83±0.05	3.5±0.1	2.9 ±0.1	1.80±0.06	1.20	0.62

*I_L, I_M and I_S are the largest, middle and smallest moments of inertia.
[a] In the interval 43.2–230 ps.
[b] In the interval 163.2–250 ps.
[c] In the interval 43.2–230 ps. These partial trajectories were chosen such that the conformation had stabilized.

A

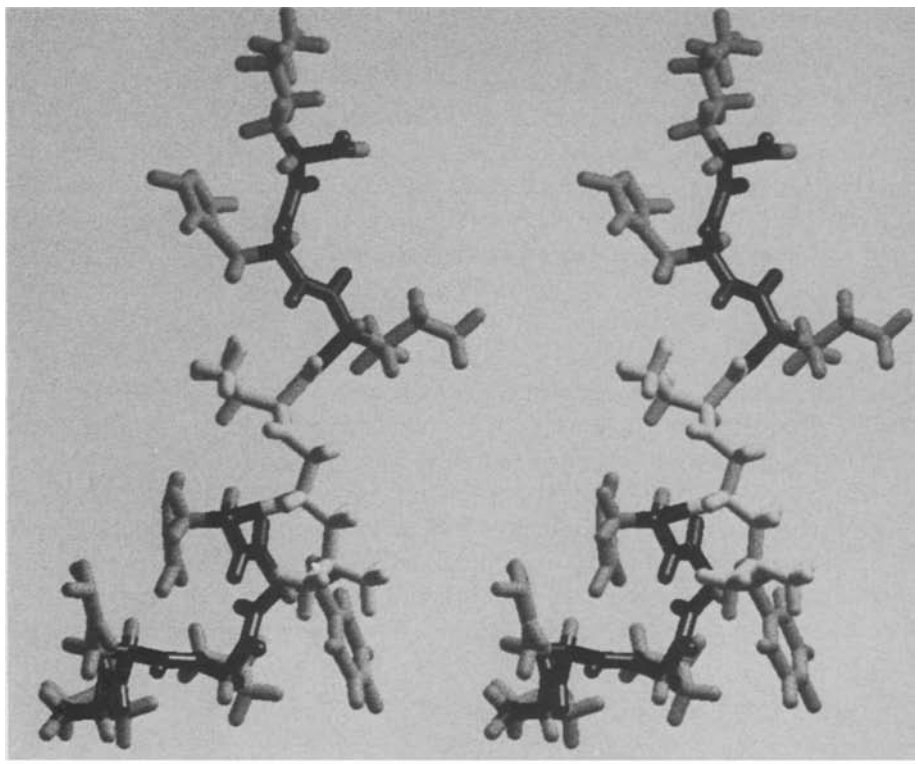

B

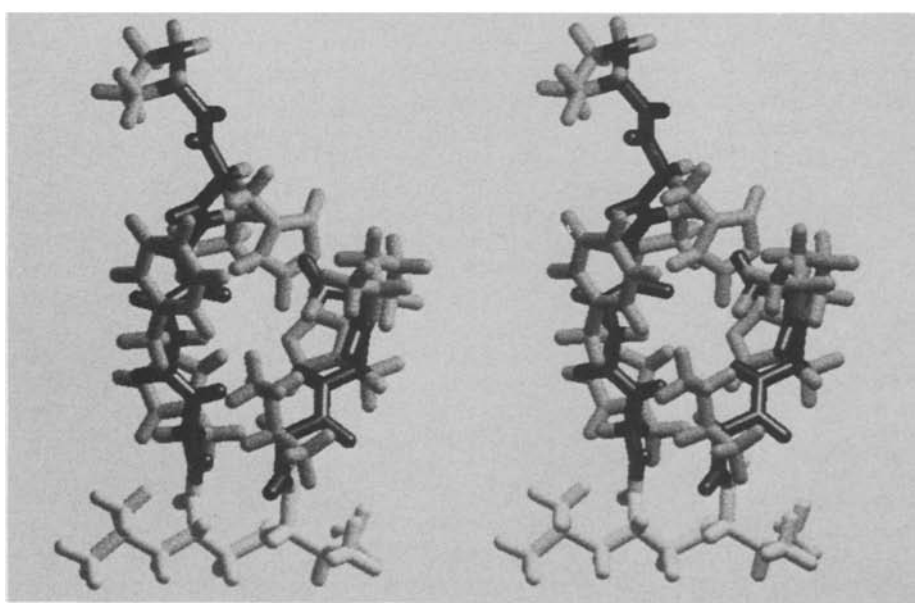

Fig. 3. Simulated conformations. A shows the conformation of H142 at the end of the H142(aq) run, t = 253 ps. B shows the same at the end of H142(80), as a representative of the continuum runs. Note that the folding is achieved by rotation around the reduced peptide bond. Shading and generation as for Fig. 1.

which compete with the intrapeptide hydrogen bonds of the folded states. These effects are normally outweighed by the even stronger solvent-solvent interactions which favour folded states. Whatever the equilibrium, folding is retarded viscously by the water, and it appears that the present water simulations are not long enough. A recent study of hydrogen bonds in a simulation of Calbindin D_{9k} [26] further indicates that the present force field underestimates intrapeptide hydrogen-bond strength and so favours unfolded states. Work is in progress in our laboratory to investigate this force-field artifact. The problem of hydrophobic interactions is particularly acute for the simulation of amphiphiles, (see e.g. Refs. 27–29).

An attempt to accelerate folding was made by raising the temperature to 600 K. Figure 2C shows r_G as a function of time, but the increased ability to pass barriers does not bring about further folding within the simulated extra 80 ps. Recooling the system to 310 K does not cause the peptide to adopt a more folded conformation.

The principal moments of inertia (see Table 3) show that the peptide is nearly spherical in the continuum simulations, but that it remains prolate in the aqueous simulations. The same can be deduced from the end-to-end distance, i. e. the distance between C_α in Pro^1 and C_α in Lys^{10}. The end-to-end distance decreases in all continuum simulations, but is a more local property than r_G. Analogous to Fig. 1, Fig. 3A shows H142 towards the end of the H142(aq) run, while Fig. 3B shows the peptide in the H142(80) run.

Structural similarity can be assessed by evaluation of large numbers of individual geometric properties, but is more easily obtained by

$$R(\text{conf. } 1|\text{conf. } 2) = \frac{\sqrt{\sum_{\text{atoms}} m_i(\mathbf{r}_{i,\text{conf. } 1} - \mathbf{r}_{i,\text{conf. } 2})^2}}{\sqrt{\sum_{\text{atoms}} m_i}}$$

which is the root-mean-square deviation at optimal rigid body superposition of two peptide conformations. Here, the sums ran over the N, C and C_α atoms of the backbone. The carbonyl oxygen was not used, in order to avoid problems with the reduced Val^6 in H142. Table 4 shows R for conformation pairs where both conformations were taken from the same trajectory, such as

$$\langle R(\text{H142(aq)(t)}|\text{H142(X-ray)})\rangle_t$$

where H142(aq)(t) means the conformation of H142 at time t in the H142(aq) simulation, and the brackets indicate a time average. The same data are visualized in Fig. 4.

As is obvious from r_G, the peptides change considerably in the continuum simulations from the X-ray conformation. This is borne out by the R values. Further, the two aqueous simulations show R values against the X-ray of about 2 Å, amounting to considerable fluctuations. R values of 2 Å are far less than those for the continuum simulations (up to 7 Å). This simply reflects folded vs. unfolded states. During the later parts of the continuum simulations, where conformations appear stable, R values against the conformation at the end of the simulation are less than 1 Å, which thus is what to expect for fluctuations around an equilibrium structure and on the 100 ps time scale.

TABLE 4
ROOT-MEAN-SQUARE DEVIATIONS WITHIN RUNS

	Low temp.	X-ray	t_0	t_{end}
H142n(v)	4.27±0.68	6.23±0.67	2.59±0.76	0.89±0.80
H142n(4)	4.21±0.28	6.37±0.26	2.56±0.38	0.64±0.29
H142n(20)	3.11±0.37	5.11±0.31	1.64±0.33	0.91±0.24
H142n(80)	2.87±0.36	4.66±0.43	1.45±0.54	2.25±0.65
H142n(aq)	3.35±0.57	2.11±0.57	2.01±0.48	1.86±0.55
H142(v)	4.51±0.52	6.71±0.99	6.45±1.16	1.16±1.09
H142(4)	3.81±0.41	6.37±0.57	3.88±0.64	0.83±0.63
H142(20)	3.49±0.36	6.35±0.58	3.71±0.66	0.73±0.66
H142(80)	2.13±0.38	4.67±0.67	1.34±0.47	1.17±0.68
H142(aq)	2.36±0.56	2.30±0.66	2.39±0.79	2.16±0.54
H142(10K)		1.58±0.54		
H142n(10K)		2.08±0.65		

All values in Å. The data shown are the RMSD between conformations out of the same trajectory, where one conformation is specified by the column head and the other is taken from the run at time t. The RMSD have been averaged over t from t=0 to t=end. In the column headed low temp., the RMSD are taken against the end conformation from the 10 K run of the same peptide.

Table 5 and Fig. 5 show $< R$ (one trajectory (t) | another trajectory (t)) $>_t$, i.e. simulations are compared. All pairs of continuum trajectories deviate at least 2 Å from each other, and thus more than could be due to minor fluctuations. In consequence, all continuum simulations produce different folding, which, because of the unnatural peptide environment in these simulations, indicates that they do not produce physically correct folding.

Expectedly, the two forms of the peptide, H142 and H142n, most resemble each other when simulated under identical conditions. R(H142(ε=x)|H142n(ε=y)) increases with increasing diffe-

TABLE 5
ROOT-MEAN-SQUARE DEVIATIONS BETWEEN RUNS

	H142n(4)	H142n(20)	H142n(80)	H142(v)	H142(4)	H142(20)	H142(80)	H142n(aq)	H142(aq)
H142n(v)	2.34±0.28	3.45±0.48	3.57±0.30	2.11±0.78	2.26±0.31	2.44±0.23	2.91±0.69	6.48±0.97	5.07±0.70
H142n(4)		2.31±0.39	3.58±0.42	2.92±0.52	1.98±0.20	1.96±0.28	2.58±0.71	6.67±0.71	5.22±1.01
H142n(20)			2.90±0.33	4.06±0.36	2.66±0.35	2.28±0.50	2.33±0.40	5.48±0.72	3.91±0.75
H142n(80)				4.55±0.97	3.19±0.43	2.80±0.40	2.97±0.39	5.03±0.68	3.94±0.60
H142(v)					2.88±0.24	3.20±0.27	3.75±0.72	6.94±1.16	5.63±0.94
H142(4)						1.63±0.29	2.88±0.57	6.65±0.96	4.97±0.93
H142(20)							2.61±0.59	6.33±1.02	4.78±0.71
H142(80)								5.41±0.86	3.64±0.74
H142n(aq)									2.85±0.91
H142(aq)									

All values in Å. The data shown are RMSD for conformation pairs, where one conformation was taken from the run to the left and the other from the run in the column head. The conformations were sampled at the same time. The RMSD were averaged over time from t=0 to t=end.

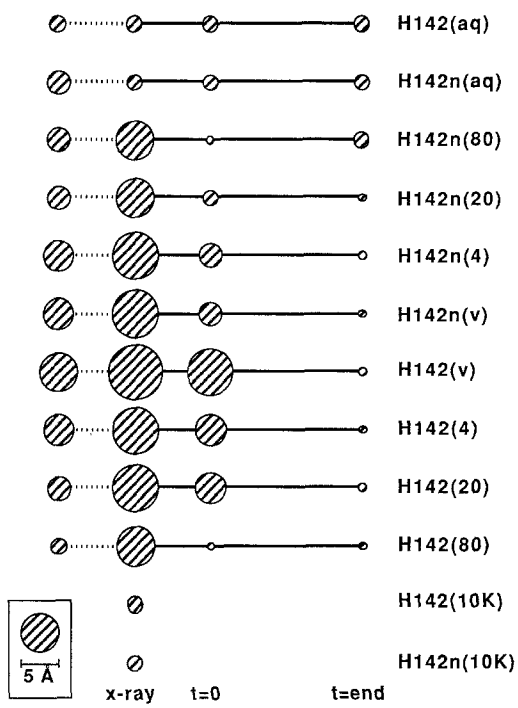

Fig. 4. Visualization of the superposition data of Table 4. The RMS deviation is shown as a hatched circle, whose diameter is proportional to the RMS value. The RMSD apply to pairs of conformations, where one conformation is specified at the bottom of the diagram and the other is taken from the same run at time t, whereupon the RMSD have been averaged over t from t = 0 to t = end. The leftmost circle for each run shows the RMSD against the end conformation from the 10 K run of the same peptide.

rence in permittivity, which applies also to R(H142($\varepsilon = x$)|H142($\varepsilon = y$)) and R(H142n($\varepsilon = x$)|H142n($\varepsilon = y$)). The conformations in solution are strongly dissimilar to all continuum conformations, with R values up to 7 Å. The dissimilarity is slightly less when comparing to the high-permittivity simulations ($\varepsilon = 80$).

Low-temperature simulations. Figure 2 and Table 4 also compare simulations to the low-temperature runs H142(min) and H142n(min). All continuum trajectories deviate substantially from the corresponding low-temperature run. Generally, R(H142($\varepsilon = x$)|H142(min)) is less than R(H142($\varepsilon = x$)|H142(X-ray)), and the same applies for H142n. Thus the changes in H142(min) and H142n(min) probably occur also at 310 K, even if they are only a minor part of the changes taking place at that temperature.

Chemical modification. In the absence of folding in H142(aq) and H142n(aq) we cannot assess the effect of chemical modification on conformation. All normal peptide bonds remain *trans* at all times. The reduced bond, ω, enjoys more flexibility. In the H142 continuum runs it settles in deformed *gauche* conformations, in H142(v) and H142(4) with $\omega < 0°$ and in H142(20) and H142(80) with $\omega > 0°$, where ω is the peptide dihedral angle C_α-C-N-C_α at Leu^6-Val^7. In H142(aq) ω starts in approximate *trans* (t = 0) but passes to *gauche* ($\omega < 0°$) and fluctuates around that for most of the trajectory.

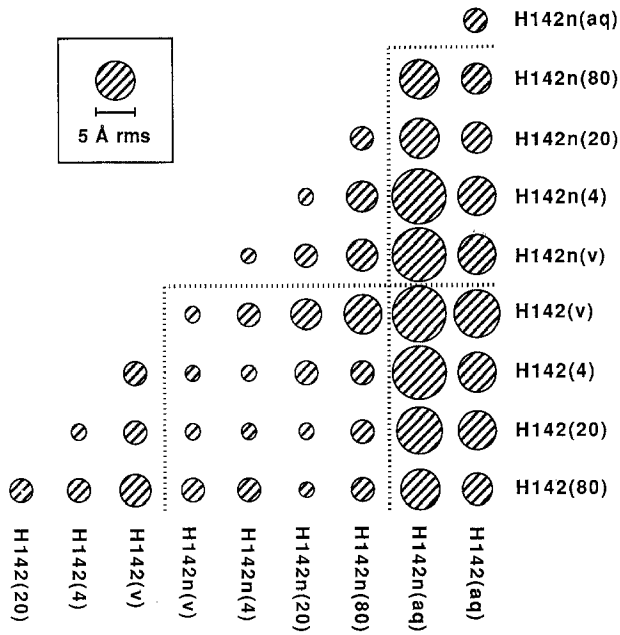

Fig. 5. Visualization of the superposition data of Table 5. The RMS deviation is shown as a hatched circle, whose diameter is proportional to the RMS value. The circles give the RMSD for conformation pairs, where one conformation was taken from the run to the right and the other from that at the bottom. The conformations were sampled at the same time, and the RMSD were averaged over time from t = 0 to t = end.

Secondary structure was evaluated by means of Ramachandran diagrams, where we plotted the Ψ angle as a function of the Φ angle for all times. Thus we obtained a secondary structure trajectory in Ψ,Φ-space (see Fig. 6). The result is given for all residues and trajectories in Table 6. The conformation in the endothiapepsin complex is all β sheet. In all cases at least one transition to either α_R or α_L occurs. In H142(ε=4), Pro^1 changes to α_R, while all other residues remain β. Nevertheless r_G decreases to 6 Å, with the backbone gently curving and all side chains clustering. The H142n(80) trajectory shows the most transitions, five, while only one occurs in each aqueous simulation.

Such transitions in secondary structure as observed here cannot be obtained by energy minimization. The MD simulation is thus a more powerful means of conformational search. Even so, brute-force simulation is not capable of generating the correct folded structure. The best model, H142(aq) and H142n(aq), cannot be simulated long enough. Distance constraints based on NOE data from NMR spectroscopy would solve this problem [30–33] but preliminary work indicates that NMR spectroscopy is difficult with H142 because of low water solubility (Maria Selander and Torbjörn Drakenberg, personal communication).

Overall dynamics. As opposed to molecular mechanics, energy minimization and Monte Carlo simulation, MD trajectories specify positions as functions of physical time so that dynamic properties are accessible. Rotation dynamics can be evaluated by means of time-correlation functions (tcf's) that describe the reorientation of some vector:

$$C_j(\Delta t) = \langle P_j[\cos\Phi(t,\Delta t)]\rangle_t$$

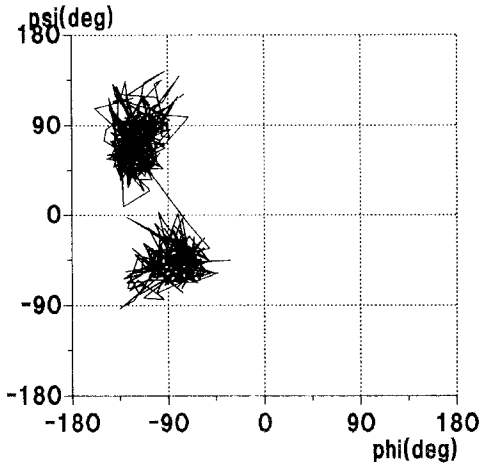

Fig. 6. Trajectory in Φ,Ψ-space for His[5] in the H142n(aq) run. There is one transition from β to α_R, which occurs approximately halfway through the trajectory. For other residues and runs, see Table 6.

where P_j is the Legendre polynomial of order j, Φ is the angle between the investigated vector at time t and at time $t+\Delta t$. A correlation time τ_j is defined by

$$\tau_j = \int_{t=0}^{\infty} C_j(t)\,dt$$

For simple stochastic processes the tcf is a single exponential, $C_j = \exp(-t/T)$ and then $\tau_j = T$. It is often possible to approximate C_j by an exponential and thus to obtain an approximation to τ_j by least-squares fitting of an exponential. We will call the correlation time of the fitted exponential the characteristic time of the real process.

TABLE 6
SECONDARY STRUCTURE

Dihedral angles	H142(v)	H142n(v)	H142(4)	H142n(4)	H142(20)	H142n(20)	H142(80)	H142n(80)	H142(aq)	H142n(aq)
$\Phi_1-\Psi_1$	β	β	α_R	β	$\beta\rightarrow\alpha_R$	β	β	β	β	β
$\Phi_2-\Psi_2$	α_L	α_L	β	β	β	β	β	$\alpha_L\rightarrow\beta$	β	β
$\Phi_3-\Psi_3$	β	β	β	β	β	β	β	β	$\beta\rightarrow\alpha_R$	β
$\Phi_4-\Psi_4$	$\beta\rightarrow\alpha_R$	β	β	β	β	$\beta\leftrightarrow\alpha_R^a$	β	β	β	β
$\Phi_5-\Psi_5$	$\beta\rightarrow\alpha_R$	$\beta\leftrightarrow\alpha_R^a$	β	α_R	α_R	α_R	β	β	β	$\beta\rightarrow\alpha_R$
$\Phi_6-\Psi_6$	β	β	β	$\beta\rightarrow\alpha_R$	β	α_R	β	$\alpha_R\rightarrow\beta$	β	β
$\Phi_7-\Psi_7$	α_R	α_R	β	β	β	β	β	$\beta\rightarrow?\rightarrow\alpha_R$	β	β
$\Phi_8-\Psi_8$	β	β	β	β	β	β	β	$?\rightarrow\alpha_R$	β	β
$\Phi_9-\Psi_9$	β	β	β	β	α_R	α_R	$\alpha_R\rightarrow\beta$	$\alpha_R\rightarrow\beta$	β	β

[a]Several transitions.

TABLE 7
CHARACTERISTIC TIMES FOR BACKBONE MOTION*

	H142(v)	H142n(v)	H142(aq)	H142n(aq)
Pro^1-His^2	0.32	0.23	0.13	0.16
His^2-Pro^3	0.36	0.87	0.10	0.11
Pro^3-Phe^4	0.35	0.18	0.22	0.12
Phe^4-His^5	0.21	1.07	0.23	0.28
His^5-Leu^6	0.11	0.48	0.19	0.24
Leu^6-Val^7	0.24	0.27	0.31	0.18
Val^7-Ile^8	0.47	0.26	0.13	0.16
Ile^8-His^9	0.34	1.36	0.26	0.22
His^9-Lys^{10}	0.38	0.70	0.082	0.14
Overall rotation			0.50	1.46

*All values in ns. The characteristic times are based on the first-order correlation function. The vector on which the backbone reorientation was based is the vector between C_α's in subsequent residues. The overall reorientation was based on the total angular momentum, as described in the main text.

The overall rotation of the peptide was based on three vectors rotated according to the total angular momentum of the peptide [34]. The time-correlation functions are shown in Fig. 7, and the least-squares fit was done between 2 and 20 ps. The overall rotation is of course exactly zero in the continuum simulations. The characteristic time τ_1 was 0.5 ns for H142 and 1.5 ns for H142n. The statistics of the overall reorientation is determined by the number of collisions with water molecules. Thus a number of 1 ns may be derived from a 250-ps simulation, but only if no modes of motion exist on intermediate time scales. For H142, we believe that some folding will occur, so that the reorientation of the present elongated conformation is not the same as for the peptide at equilibrium. The H142 rotation is slower than that of Substance P, a peptide of similar size, which assumed a folded conformation in a simulation by Teleman and v. d. Lieth [35].

The translational diffusion was evaluated from the mean-square displacement of the peptide

TABLE 8
CHARACTERISTIC TIMES FOR SIDE-CHAIN MOTION*

	H142(v)	H142n(v)	H142(aq)	H142n(aq)
Pro^1:$C_\beta \rightarrow C_\delta$	0.17	0.16	0.054	0.040
His^2:$N_{\delta 1} \rightarrow N_{\varepsilon 2}$	0.18	0.15	0.038	0.038
Pro^3:$C_\beta \rightarrow C_\delta$	0.29	1.10	0.078	0.078
Phe^4:$C_{\varepsilon 1} \rightarrow C_{\varepsilon 1}$	0.21	0.15	0.054	0.083
His^5:$N_{\delta 1} \rightarrow N_{\varepsilon 2}$	0.093	0.046	0.12	0.068
Leu^6:$C_\gamma \rightarrow C_{\delta 1}$	0.43	0.61	0.19	0.11
Val^7:$C_\beta \rightarrow C_{\gamma 1}$	0.31	0.26	0.092	0.085
Ile^8:$C_{\gamma 1} \rightarrow C_{\delta 1}$	0.26	0.25	0.084	0.083
His^9:$N_{\delta 1} \rightarrow N_{\varepsilon 2}$	0.13	0.21	0.075	0.066
Lys^{10}:$C_\varepsilon \rightarrow N_\zeta$	0.055	0.087	0.028	0.10

*All values in ns. The characteristic times are based on the first-order correlation function.

centre of mass. The diffusion coefficient is obtained as

$$D = \lim_{\Delta t \to \infty} \frac{1}{6\Delta t} <[\mathbf{r}(t+\Delta t) - \mathbf{r}(t)]^2>_t$$

where **r** is the position of the centre of mass. The diffusion coefficient, which is meaningful only in the aqueous simulations, was found to be 4.6×10^{-10} m^2/s (H142) and 3.1×10^{-10} m^2/s (H142n). The values are similar to the one obtained for Substance P [35].

Local dynamics. Local motion in the backbone was described by tcf's for vectors connecting sequentially adjacent C_α atoms. The first-order characteristic times are given in Table VII for four of the trajectories. In the vacuum simulations characteristic times are as long as 1.4 ns occasionally, while the solvent in the H142(aq) and H142n(aq) runs induces more motion also locally.

Side-chain motion was evaluated for vectors at the end of each side chain, as listed in Table VIII together with characteristic times. Again, some vectors are nearly immobilized in the H142n(v) run, which shows up as very long characteristic times. In the aqueous trajectories side-chain motion is faster than backbone motion, which reflects that side chains enjoy more flexibility and are more affected than the backbone by the collisions with water molecules.

Hydrogen bonds. Hydrogen bonds were evaluated using an asymmetric criterion such that a hydrogen bond is considered to be formed when the hydrogen-acceptor distance becomes less than 3.2 Å and the donor-hydrogen-acceptor angle at the same time exceeds 135°. The bond is deemed to cease when either the distance exceeds 3.6 Å or the angle becomes less than 100°. The reason for the asymmetry is that unfavourable encounters may not result in a hydrogen bond while, on the other hand, a bond already formed may vibrate and occasionally be very long without actually breaking. Linse et al. [26] discuss hydrogen-bonding criteria.

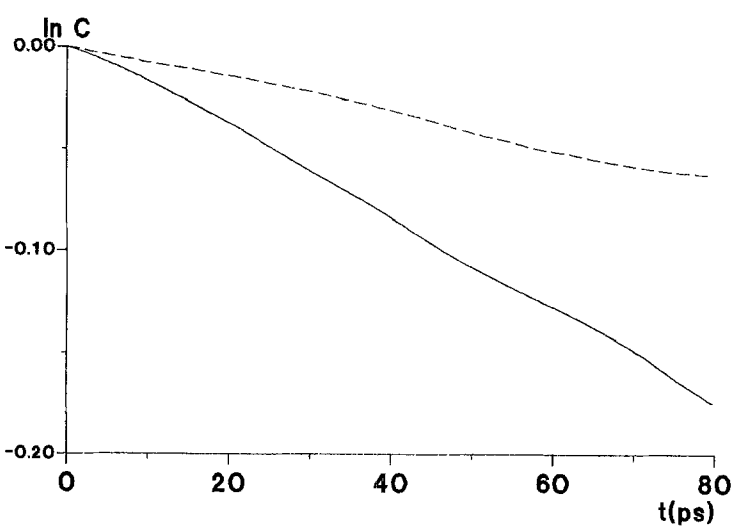

Fig. 7. Logarithms of first-order time correlation functions for the overall reorientation of H142 and H142n in aqueous solution. The values given in Table 7 for the characteristic times are derived from linear fits to these curves between 2 and 20 ps.

Only a few intramolecular hydrogen bonds last longer than 1 ps. In the H142(aq) run there are only two, one between O in His^5 and NH in Val^7 (1 ps) and one between $N_{\varepsilon 2}$ in His^9 and $H_{\xi 2}$ in Lys^{10} (5 ps). In the H142n(aq) trajectory four hydrogen bonds were found. $H_{\delta 1}$ in His^5 binds O in His^2 (1 ps) and O in Pro^3 (5 ps), NH in Leu^6 binds to O in Phe^4 (1 ps) and H in Val^7 binds O in His^5 (5 ps).

The peptide-water hydrogen bonds were many but also short-lived. Out of 1362 hydrogen bonds in the H142(aq) run, only 7 lasted longer than 15 ps, with the longest (21 ps) involving a carboxyterminal oxygen. Similarly, only 19 out of 1685 hydrogen bonds in the H142n(aq) trajectory were longer-lived than 15 ps, with the terminal carboxyl again taking part in the longest-lived (31 ps).

The scarcity of intramolecular hydrogen bonds is partly due to the elongated conformation. The backbone atoms that potentially take part in hydrogen bonds are not in a favourable position to do so. The same applies to the side chains containing such atoms, His^2, His^5, His^9 and Lys^{10}. The opposite situation occurred in the simulation of an 11-residue peptide in a folded state (Substance P, [35]), where 307 hydrogen bonds longer-lived than 1 ps were found.

Discussion of cost vs. benefit. The industrial theoretical chemist may ask whether MD pays off, even if it is the *non plus ultra* in modelling. The bare truth, however, is that most problems cannot be handled even at today's state-of-the-art level. MD delivers a wealth of data, but deals best with local structure and fast processes and thus best with problems where detailed information is important. In a larger perspective, MD is undoubtedly at its best in conjunction with experimental data, such as NOE distance constraints to ensure correct global properties. The two crucial limitations are the sampling of phase space, i. e. simulation length, and force-field accuracy. Better force fields may be developed in the next few years following advances in quantum chemistry, while sampling improves with ever-increasing computer performance. The choice of modelling approach depends on the problem, but where a coarser method is chosen, reassessment should not be too infrequent.

CONCLUSION

Performed simulations model the initial behaviour of H142 and H142n on release from endothiapepsin. The MD simulations search a larger part of phase space than is accessible by energy minimization techniques. Continuum environments have been shown to be unrealistic for a wide range of permittivity values. The expected hydrophobic folding does not occur in the simulations of aqueous solutions. This indicates either that simulations are too short, or that the force field artificially favours the extended state, or that the real peptide actually remains in an extended state.

ACKNOWLEDGEMENTS

We would like to thank Supercomputer Centre North, Sweden (SDCN) for generous allocation of computer time. We are also grateful for access to the graphics package WINSOM, written by the IBM Scientific Centre at Winchester, U.K. O. T. wishes to acknowledge a grant by the Swedish Natural Science Research Council. Erik Johansson, Hässle AB, is gratefully acknowledged for providing the coordinates of H142 in the endothiapepsin complex.

REFERENCES

1 Foundling, S.I., Cooper, J., Watson, F.E., Pearl, L.H., Hemmings, A., Wood, S.P., Blundell, T., Hallett, A., Jones, D.M., Suciras, J., Atrash, B. and Szelke, M., J. Cardiovasc. Pharmacol., 10(7) (1987) S59.
2 Van Gunsteren, W.F. and Karplus, M., Biochemistry, 21 (1982) 2259.
3 Van Gunsteren, W.F. and Berendsen, H.J.C., J. Mol. Biol., 176 (1984) 559.
4 Wong, C.F. and McCammon, A., Isr. J. Chem., 27 (1986) 211.
5 Levitt, M. and Sharon, R., Proc. Natl. Acad. Sci. USA, 85 (1988) 7557.
6 Ahlström, P., Teleman, O., Kördel, C.-J., Forsén, S. and Jönsson, B., Biochemistry, 28 (1989) 3205.
7 Rossky, P.J. and Karplus, M., J. Am. Chem. Soc., 101 (1979) 1913.
8 Brady, J. and Karplus, M., J. Am. Chem. Soc., 107 (1985) 6103.
9 Hagler, A.T., Osguthorpe, D.J., Dauber-Osguthorpe, P. and Hempel, J.C., Science, 227 (1985) 1309.
10 Hagler, A.T., Peptides, 7 (1985) 213.
11 Hagler, A.T., Strutters, R.S., Solmajer, T.J., Campbell, K.B., Tanaka, G. and Rivier, J., Pharmacochem. Libr., 10 (QSAR Drug Des. Toxicol.) (1987) 231.
12 Kitson, D.H. and Hagler, A.T., Biochemistry, 27 (1988) 5246.
13 Anderson, A., Carson, M. and Hermans, J., Ann. NY Acad. Sci., 482 (1986) 51.
14 Ahlström, P., Teleman, O., Jönsson, B. and Forsén, S., J. Am. Chem. Soc., 109 (1987) 1541.
15 Teleman, O., Ahlström, P. and Jönsson, B., Mol. Simul., (1990) in press.
16 Hermans, J., Berendsen, H.J.C., Van Gunsteren, W.F. and Postma, J.P.M., Biopolymers, 23 (1984) 1513.
17 Van Gunsteren, W. F. and Karplus, M., Macromolecules, 15 (1982) 1528.
18 Margenau, M. and Kestner, N. R., Theory of Intermolecular Forces, Pergamon, NewYork, 1969.
19 Berendsen, H.J.C., Postma, J.P.M., Van Gunsteren, W.F. and Hermans, J., In Pullman, B. (Ed.) Intermolecular Forces, D. Reidel, Dordrecht, 1981, pp. 331–342.
20 Teleman, O., Jönsson, B. and Engström, S., Mol. Phys., 60 (1987) 193.
21 Dolphin, D. and Wick, A.E., Tabulation of Infrared Data, Wiley Interscience, New York, 1977.
22 Herzberg, G., Molecular Spectra and Molecular Structure: Infrared and Raman Spectra of Polyatomic Molecules, Van Nostrand, Princeton, NJ, 1945.
23 Teleman, O. and Jönsson, B., J. Comp. Chem., 7 (1986) 58.
24 Wallqvist, A. and Teleman, O., Mol. Phys., (1990) in press.
25 Teleman, O., Jönsson, B. and Svensson, B., Comp. Phys. Comm., (1990) in press.
26 Linse, S., Drakenberg, T. and Teleman, O., Biochemistry, 29 (1990) 5925.
27 Egberts, E., Doctoral thesis, Groningen University, 1988.
28 Jönsson, B., Edholm, O. and Teleman, O., J. Chem. Phys., 85 (1986) 2259.
29 Watanabe, K., Ferrario, M. and Klein, M., J. Phys. Chem., 92 (1988) 819.
30 Braun, W. and Gō, N., J. Mol. Biol., 186 (1985) 611.
31 Havel, T. F., Kuntz, I. D. and Crippen, G. M., Bull. Math. Biol., 45 (1983) 665.
32 De Vlieg, J., Boelens, R., Scheek, R. M., Kaptein, R. and Van Gunsteren, W. F., Isr. J. Chem., 27 (1986) 181.
33 Nilges, M., Gronenborn, A.M., Brünger, A.T. and Clore, G.M., Prot. Eng., 2 (1988) 27.
34 Teleman, O., J. Comp. Chem., 11 (1990) 64.
35 Teleman, O. and v.d. Lieth, C.-W., Biopolymers, 30 (1990) 13.